# Longitudinally resolved measurement of energy-transfer efficiency in a plasma-wakefield accelerator

L. Boulton,[1,2,3,*] C. A. Lindstrøm,[1] J. Beinortaite,[1,4] J. Björklund Svensson,[1] J. M. Garland,[1] P. González Caminal,[1,5] B. Hidding,[2,3] G. Loisch,[1] F. Peña,[1,5] K. Põder,[1] S. Schröder,[1] S. Wesch,[1] M. Wing,[1,4] J. C. Wood,[1] J. Osterhoff,[1] and R. D'Arcy[1]

[1]*Deutsches Elektronen-Synchrotron DESY, Notkestrße 85, 22607 Hamburg, Germany*
[2]*SUPA, Department of Physics, University of Strathclyde, Glasgow, United Kingdom*
[3]*The Cockcroft Institute, Daresbury, United Kingdom*
[4]*Department of Physics and Astronomy, University College London, United Kingdom*
[5]*Department of Physics, Universität Hamburg, Luruper Chaussee 149, 22761 Hamburg, Germany*

(Received 1 September 2022; accepted 29 April 2026; published 1 June 2026)

Energy-transfer efficiency is an important quantity in plasma-wakefield acceleration, especially for applications that demand high average power. Conventionally, the efficiency is measured using an electron spectrometer, an invasive method that provides an energy-transfer efficiency averaged over the full length of the plasma accelerator. Here, we experimentally demonstrate the use of the excess light emitted by the plasma after a beam-plasma interaction in a method that yields noninvasive, longitudinally resolved measurements of the local energy-transfer efficiency from the wake to the accelerated bunch. As we show, by diagnosing the acceleration process directly at the plasma location, this method can provide more insight into effects such as trailing bunch charge loss, which typically impose systematic errors on downstream spectrometer measurements. In the future, this method would also be suitable for the online optimization of individual stages in multistage plasma accelerators.

DOI: 10.1103/b8hj-shvc

With the promise of gigavolts-per-meter accelerating gradients [1–3], plasma wakefields driven by intense laser [4] or particle beams [5,6] offer a path toward compact accelerators for high-energy physics [7] and photon science. In a beam-driven plasma-wakefield accelerator (PWFA), energy is transferred from a driver to the plasma by expelling plasma electrons from its path; some of this energy can subsequently be extracted by a trailing particle bunch placed at the correct distance behind the driver. Trailing bunches with a sufficiently high current can alter the trajectory of the expelled plasma electrons as they return to the axis, modifying the local accelerating field while efficiently extracting energy from the wake [8–10]. This effect, known as *beam loading* [11,12], has been used to demonstrate energy-transfer efficiencies from the wake to the trailing bunch of up to 42% ± 4% in PWFA, while simultaneously preserving beam properties such as charge and energy spread [13–15].

Traditionally, energy-transfer efficiency is measured using magnetic dipole spectrometers by comparing the energy loss and gain of the driver and trailing bunch, respectively. These measurements are longitudinally averaged over the full plasma stage, are invasive due to scattering of the charge by the diagnostic screen, and require stable, multishot measurements with varying beam imaging in order to ensure high-energy resolution. As a result, experimental optimization is slow and precludes simultaneous spectrometer-based measurements of efficiency in individual stages of a future multistage plasma accelerator [16,17].

In this article, we present a method of measuring the energy-transfer efficiency of a plasma accelerator by detecting plasma-emission light from the dissipation of residual energy in the plasma wake. Previous work has introduced plasma-emission light as a simple, nondestructive observable of the strength of a beam-plasma interaction [18,19], which was also used for alignment and synchronization [20–22] and has more recently served as a simple diagnostic of the unperturbed plasma itself [23,24]. Here, we observe not only an increased light yield in the presence of a beam driver but also a reduction when a trailing bunch extracts energy from the wake. By measuring the wake-energy-versus-plasma-light response curve, energy-transfer efficiency can thereby be inferred directly from the plasma light. Importantly, this signal can be measured with high spatial resolution, enabling longitudinally resolved measurements of efficiency along the plasma accelerator.

## I. EXPERIMENTAL SETUP

Observations of this effect took place at the FLASHForward plasma-accelerator facility at DESY [25]. The FLASH linac [26] provided electron bunches from a photocathode that were accelerated to a mean electron energy of 1050 MeV

*Contact author: lewis.boulton@desy.de

*Published by the American Physical Society under the terms of the Creative Commons Attribution 4.0 International license. Further distribution of this work must maintain attribution to the author(s) and the published article's title, journal citation, and DOI.*

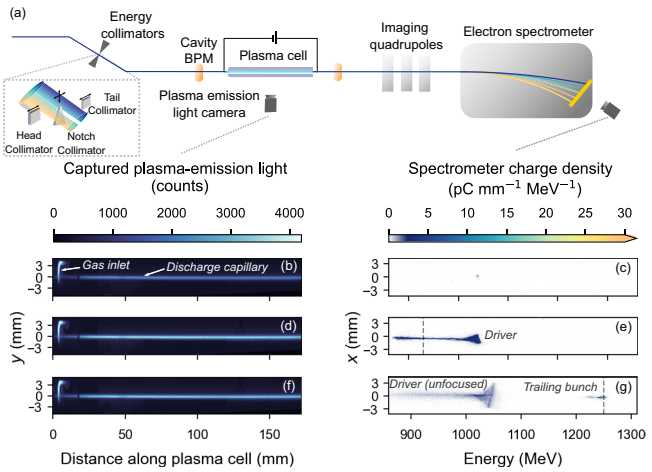



FIG. 1. (a) Generated via energy collimators in a horizontally dispersive section, a driver-trailing bunch pair was focused into a plasma before being diagnosed by a vertically dispersive imaging electron spectrometer. Meanwhile, the light emitted by the plasma was measured by a camera observing the side of the cell. Corresponding images of the plasma-emission light and spectrometer screen are shown for three representative shots: (b), (c) negligible beam charge; (d), (e) driver bunch only; and (f), (g) both the driver and trailing bunch. The imaging energy (dashed lines in spectrometer images) was optimized to resolve the relevant parts of the spectrum. Note that in the plasma-emission light images, a quadratic color scale is used to highlight differences at high counts.

(known to within 1% systematic error). The bunches delivered to the FLASHForward beamline [see Fig. 1(a)] were compressed to a root-mean-square (rms) bunch length of 300 μm and linearly chirped in longitudinal phase space, as measured by an *X*-band transverse deflecting cavity [27]. A triplet of energy collimators in a dispersive section provided control over the current profile [28]: a notch collimator for generating a driver and trailing bunch, as well as head and tail collimators for adjusting their respective charges. The bunches were focused [29] at the entrance of a 195-mm-long, 1.5-mm-diameter cell, comprised of two milled sapphire slabs with gas inlets located 2.5 mm from either end [30,31]. Plasma was generated by discharging high-voltage pulses through the cell, which was filled with argon gas at a pressure of 9 mbar. A 3% hydrogen dopant also enabled plasma-density measurements via observations of the H-alpha spectral line broadening with an optical spectrometer [31,32]. By allowing the initial plasma to decay, the plasma density experienced by the bunches could be precisely controlled. The density in the flattop region of the plasma 9.64 μs after the start of the discharge was measured to be approximately $(5.6 \pm 0.3) \times 10^{15}\,\mathrm{cm}^{-3}$. A complementary metal-oxide semiconductor camera (Basler ace GigE acA2040-25gmNIR) also provided spatially resolved measurements of the plasma-emission light radiated through one side of the plasma cell [Figs. 1(b), 1(d), and 1(f)]. Finally, five quadrupole magnets were used to transport the outgoing electron bunches through a dipole spectrometer to a LANEX screen, onto which the beams were point-to-point imaged from the end of the plasma source [Figs. 1(a)–1(c)].

## II. HIGH ENERGY-TRANSFER EFFICIENCY WORKING POINT

An operating point for high energy-transfer efficiency plasma acceleration in the nonlinear regime, as shown in Fig. 1(g), was found by following the optimization technique described in Ref. [15]. Since the energy resolution of the electron spectrometer decreases away from the imaging energy, accurate spectral measurements of the two bunches cannot occur simultaneously. Imaging at an energy of 930 MeV, the measured mean energy decrease of the driver electrons was $\Delta E_{\mathrm{dec}} = 69 \pm 3$ MeV, where the quoted uncertainty refers to the rms over the given shots. The average driver charge measured at the calibrated screen [33] was $340 \pm 7$ pC—6 % lower than that measured in the pre- and post-plasma beam position monitors (BPMs), where the charge was $360 \pm 8$ pC. As discussed in detail in Ref. [34], this charge is lost in the postplasma transport and its energy is unknown, resulting in a systematic error on the total driver energy loss. In the simplest case, which will be used here as standard, this missing charge is assumed to be distributed evenly across the driver spectrum such that the total driver energy loss is $\Delta W_{\mathrm{dec}} = Q_{\mathrm{dec}} \Delta E_{\mathrm{dec}} = 25 \pm 2$ mJ, where $Q_{\mathrm{dec}}$ is the integrated charge in the corrected driver spectra. Lower and upper bounds on $\Delta W_{\mathrm{dec}}$ can also be estimated by considering the cases where either this missing charge experienced no energy loss or the maximum energy loss observed, resulting in total driver energy losses of $23 \pm 1$ and $27 \pm 2$ mJ, respectively. The effects of this systematic uncertainty on the results that follow are discussed where appropriate.

Charge loss of the driver is primarily due to the chromatic postplasma transport of high-energy spread beams. Trailing bunches, on the other hand, while in this case having per-mille level energy spread, are much more sensitive to the acceleration process. Located at the back of the wake, these bunches are prone to experience the defocusing fields in the cavity walls and strong transverse kicks. This can result in charge loss within the plasma and/or the postplasma transport. To have a fairer comparison with the method presented in this paper, only trailing bunches with the highest 10 % of charge measured on the spectrometer were considered. For these trailing bunches, the mean electron energy gain, charge, and total energy gain were $\Delta E_{\mathrm{acc}} = 194 \pm 4$ MeV, $Q_{\mathrm{acc}} = 44 \pm 1$ pC, and $\Delta W_{\mathrm{acc}} = Q_{\mathrm{acc}} \Delta E_{\mathrm{acc}} = 8.4 \pm 0.2$ mJ, respectively. Using the total energy loss of the driver that was separately measured, the resulting mean energy-transfer efficiency for these shots, defined by

$$\eta_{\mathrm{s}} = \frac{\Delta W_{\mathrm{acc}}}{\Delta W_{\mathrm{dec}}}, \tag{1}$$

was calculated to be $34\% \pm 2\%\%$, with lower and upper bounds due to the systematic error on $\Delta W_{\mathrm{dec}}$ of $31\% \pm 2\%$ and $36\% \pm 2\%$, respectively.

In addition, the overall driver-to-trailing bunch energy-transfer efficiency can also be calculated for these shots, defined as $\frac{\Delta W_{\mathrm{acc}}}{W_{\mathrm{dec}}}$, where $W_{\mathrm{dec}}$ is the total energy of the incoming driver. Using the driver-only charge from the preplasma BPM and the incoming driver electron energy results in $W_{\mathrm{dec}} = 378 \pm 10$ mJ and therefore a driver-to-trailing bunch

energy-transfer efficiency of $2.2\% \pm 0.1\%$. This represents a significant improvement over the previous high-efficiency working point detailed in Ref. [15], where, despite accelerating 2.2 times as much trailing bunch charge on average, the driver-to-trailing bunch energy-transfer efficiency was $0.9\% \pm 0.1\%$. A higher overall efficiency in the results reported here is owed partially to the use of a lower incoming driver charge, but predominantly to the longer plasma that results in approximately 4 times the trailing bunch energy gain.

## III. MEASURING WAKE ENERGY WITH PLASMA-EMISSION LIGHT

Plasma-emission light was measured simultaneously with the spectral measurements, detected by the camera imaging the side of the plasma cell. No spectral filtering of the light was used, and the quantum efficiency of the camera chip varied slowly between ~400 and 800 nm. The light signal, captured with a 24 μs exposure window starting immediately after beam arrival, was observed to vary with the current profile of the incoming beam, which was adjusted using the tail collimator in the dispersive section. Beginning with the collimator completely inserted [Fig. 1(c)], the light captured was primarily that from the discharge plasma with negligible beam interaction [Fig. 1(b)]. Partially extracting the collimator until only the driver reached the plasma [Fig. 1(e)] resulted in a substantial increase in the captured light [Fig. 1(d)]; as the driver decelerated, energy was transferred to the plasma wake. This additional energy was eventually dissipated into the bulk plasma, some of which was emitted as excess plasma-emission light. When the collimator was further extracted such that a trailing bunch was introduced [Fig. 1(g)], the excess plasma-emission light was observed to decrease [Fig. 1(f)]. This occurred because the trailing bunch extracted energy from the wake, making the reduction in plasma-emission light a simple signature of the energy that remained in the plasma wake. Figure 2 demonstrates this effect in more detail. By progressively increasing the amount of driver charge [Fig. 2(a)], the correlation between the total energy lost by the driver and the resulting excess light yield was established [Fig. 2(b)]. Here, the light is integrated spatially along the plasma accelerator. To account for any longitudinal variation in light-collection efficiency across the field of view, the light signal from a uniform plasma—measured with the falling edge of the camera exposure placed promptly after plasma ignition—provided a correction factor for each position along the length of the cell. The response curve is affected by the specific conditions of the experiment: The light yield depends on the optical setup and the sensitivity of the camera chip, their spectral bandwidth and attenuation, and the exposure-time settings. Changes in the plasma density—which over the duration of this experiment was approximately constant—may also require recalibration of the response curve. We note that the physical mechanism connecting the deposited energy to the emission light is currently not fully understood, as this relates to processes that occur over multiple microseconds [35,36]. At the level of this study, however, this is not necessary. All that is needed is a signal from the plasma light that can be correlated with the energy

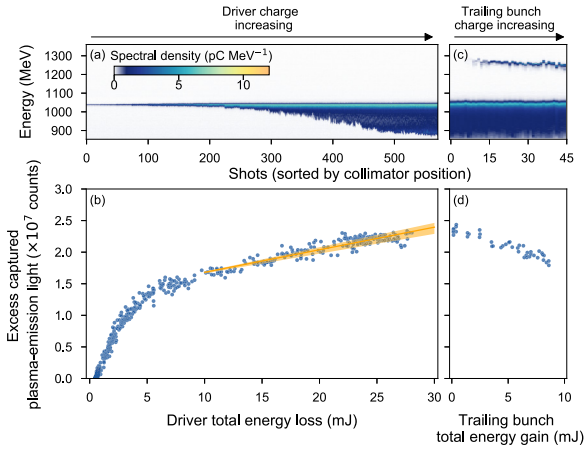



FIG. 2. (a) Driver spectra measured as the collimator is extracted, introducing more charge to the plasma wake. (b) Plasma-emission light increases with increasing total driver energy loss (blue points). A linear fit (orange line) to the points with $\Delta W_{\mathrm{dec}} > 10$ mJ is shown, with the surrounding shaded region representing the error on this fit due to the systematic uncertainty in $\Delta W_{\mathrm{dec}}$. (c) Further extracting the collimator, spectra of the trailing bunch show an increase in charge. (d) The plasma-emission light decreases as the trailing bunch extracts energy from the plasma.

deposited in the plasma, such that a calibration can be made. This calibration then allows us to estimate how much excess energy is deposited in the plasma wake based solely on the plasma-emission light.

Gradually introducing the trailing bunch [Fig. 2(c)], plasma-emission light was measured as a function of the total energy gained [Fig. 2(d)]. To reduce the systematic error due to imperfect charge coupling, again only shots with more than 90% of the maximum measured trailing bunch charge at each collimator position are considered. In the corresponding region of the light-versus-energy-loss measurement [above $1.65 \times 10^7$ counts in Fig. 2(b)], a linear fit can be used to model the plasma-emission light yield $I_{\mathrm{p}} = f(\Delta W_{\mathrm{wake}})$, where $\Delta W_{\mathrm{wake}}$ is the energy deposited in the plasma wake, equal to $\Delta W_{\mathrm{dec}}$ when only the driver is present. The previously discussed systematic uncertainty on $\Delta W_{\mathrm{dec}}$ will also introduce an error on the response curve—the resulting upper and lower bounds of this error are represented by the orange shaded region in Fig. 2(b).

The remaining wake energy can be estimated from the excess plasma-emission light by inverting the previously established model

$$\Delta W_{\mathrm{wake}} = \Delta W_{\mathrm{dec}} - \Delta W_{\mathrm{acc}} = f^{-1}(I_{\mathrm{p}}). \tag{2}$$

Equation (2) provides an alternative way of calculating energy-transfer efficiency. The total energy gained by the trailing bunch can be inferred from the plasma-emission light via $\Delta W_{\mathrm{acc}} = \Delta W_{\mathrm{dec}} - f^{-1}(I_{\mathrm{p}})$, which requires a measurement of the response curve $f$ [Fig. 2(b)] and the total driver energy loss. Substituting this into Eq. (1), the energy-transfer efficiency can be expressed as

$$\eta_{\mathrm{p}} = 1 - \frac{\Delta W_{\mathrm{wake}}}{\Delta W_{\mathrm{dec}}} = 1 - \frac{f^{-1}(I_{\mathrm{p}})}{\Delta W_{\mathrm{dec}}}. \tag{3}$$

## IV. ESTIMATING TOTAL DRIVER ENERGY LOSS DURING TRAILING BUNCH MEASUREMENTS

Note that, in both Eqs. (1) and (3), one still requires a measurement of $\Delta W_{\mathrm{dec}}$. However, while optimally imaging the trailing bunch—necessary for the most accurate measurement of $\eta_{\mathrm{s}}$—the spectrum of the driver cannot be simultaneously measured with high accuracy. Although an option is to assume that $\Delta W_{\mathrm{dec}}$ calculated from a properly imaged driver applies constantly across all shots in the trailing bunch measurements, drifts within and between these datasets, as well as the desire for a shot-to-shot comparison between the spectrometer and plasma-light-based measurements, make this estimate insufficient. Instead, using data from the beginning of the trailing bunch measurement, the total driver energy loss here was estimated from the mean plasma-emission light yield when only the driver was present $\langle I_{\mathrm{p}}\rangle_0$ [leftmost shots in Figs. 2(c) and 2(d)], where $\langle\rangle$ denotes an average over multiple shots. This provides an initial estimate of $\Delta W_{\mathrm{dec}}$ when inserted into the response curve, i.e., $f^{-1}(\langle I_{\mathrm{p}}\rangle_0)$, but can be further improved. Although calculations of the total driver energy loss from the improperly imaged driver are not perfectly accurate, they can be used to partially correct for relative shot-to-shot drifts and jitters in the driver deceleration. This assumes that charge loss due to imperfect imaging is uniform across the driver spectrum, such that its normalized shape is not affected. For an improperly imaged driver, the relative change of $Q_{\mathrm{dec}}\Delta E_{\mathrm{dec}}$ measured on the spectrometer with respect to its value when only the driver was present, $\langle Q_{\mathrm{dec}}\Delta E_{\mathrm{dec}}\rangle_0$, can be used as a correction factor for the driver energy loss estimated by $f^{-1}(\langle I_{\mathrm{p}}\rangle_0)$, resulting in a best estimate for the shot-to-shot total driver energy loss of

$$\Delta W_{\mathrm{dec}} \approx f^{-1}(\langle I_{\mathrm{p}}\rangle_0)\frac{Q_{\mathrm{dec}}\Delta E_{\mathrm{dec}}}{\langle Q_{\mathrm{dec}}\Delta E_{\mathrm{dec}}\rangle_0}. \tag{4}$$

For consistency, the same value of $\Delta W_{\mathrm{dec}}$ is used in Eqs. (1) and (3) for subsequent comparisons of $\eta_{\mathrm{p}}$ and $\eta_{\mathrm{s}}$. Due to correlated changes in the $Q_{\mathrm{dec}}$ and $\Delta E_{\mathrm{dec}}$ of the driver, there were shot-to-shot jitters on the level of 3 % rms in the value of $Q_{\mathrm{dec}}\Delta E_{\mathrm{dec}}$, as well as an overall average decrease of around 12 % as more trailing bunch charge was introduced. Using Eq. (4), these variations were corrected for in the value of $\Delta W_{\mathrm{dec}}$.

It is worth stressing here that this correction is only needed where the driver cannot be properly imaged. In this case, this was because priority was given to measuring the trailing bunch with high accuracy for the comparisons between $\eta_{\mathrm{s}}$ and $\eta_{\mathrm{p}}$ that are to follow. Indeed, a key feature of the plasma-light-based diagnostic is that a measurement of the trailing bunch is no longer needed when making efficiency calculations; spectrometer measurements could therefore prioritize the measurement of $\Delta W_{\mathrm{dec}}$. This would yield improvements in the accuracy of the plasma-light-based method compared to the demonstration presented here. Moreover, this would give the plasma-light-based method a distinct advantage to the pure-spectrometer-based method used here, where without the ability to properly diagnose the driver and trailing bunch separately, one must rely on estimates of $\Delta W_{\mathrm{dec}}$ for shot-to-shot calculations of $\eta_{\mathrm{s}}$, either from previously acquired data or from corrections like that in Eq. (4).

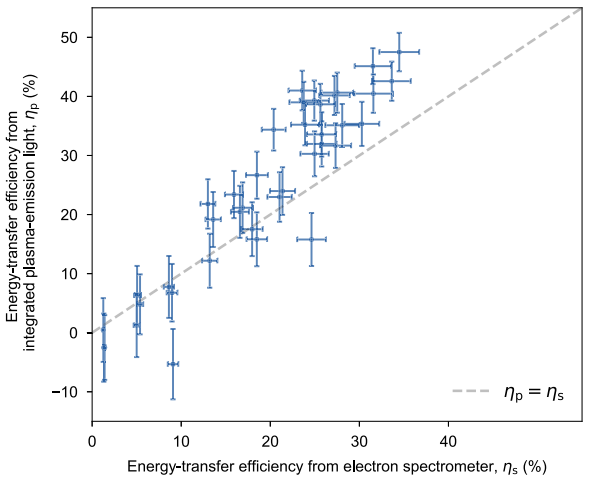



FIG. 3. Comparison of the longitudinally averaged energy-transfer efficiency measured using the plasma-emission light and the electron spectrometer for the shots shown in Figs. 2(c) and 2(d). The imperfect agreement between $\eta_{\mathrm{p}}$ and $\eta_{\mathrm{s}}$ can be explained by trailing bunch charge loss. Negative efficiencies here are due to shot-to-shot jitter in driver energy loss, resulting in some shots with $I_{\mathrm{p}} > \langle I_{\mathrm{p}}\rangle_0$ and/or $Q_{\mathrm{dec}}\Delta E_{\mathrm{dec}} < \langle Q_{\mathrm{dec}}\Delta E_{\mathrm{dec}}\rangle_0$.

## V. COMPARING SPECTROMETER- AND PLASMA-LIGHT-BASED EFFICIENCY MEASUREMENTS

Figure 3 shows a comparison of energy-transfer efficiencies calculated with the spectrometer and plasma-light-based methods, using the shots in Fig. 2(d). In both measurements, the main sources of error arise from the fit error on the model $f$, as well as the uncertainty on $\Delta W_{\mathrm{dec}}$, which receives contributions from the calculations of $\langle Q_{\mathrm{dec}}\Delta E_{\mathrm{dec}}\rangle_0$ and $\langle I_{\mathrm{p}}\rangle_0$ [Eq. (4)]. Here, the measurements are linearly correlated, but a disagreement still exists. Particularly, at higher efficiencies, the points lie above/to the left of the line $\eta_{\mathrm{p}} = \eta_{\mathrm{s}}$, where shots that have $\eta_{\mathrm{p}} > 30\,\%$ have $\eta_{\mathrm{s}}$ values that are on average 9.7 percentage points smaller than their calculated $\eta_{\mathrm{p}}$. The points in Fig. 3 instead fit best to the line $\eta_{\mathrm{p}} = 0.75\eta_{\mathrm{s}}$. At the absolute upper and lower bounds of the systematic response curve uncertainty on the response curve shown in Fig. 2(b), this becomes $\eta_{\mathrm{p}} = 0.65\eta_{\mathrm{s}}$ and $\eta_{\mathrm{p}} = 0.81\eta_{\mathrm{s}}$, respectively, and so do not fully account for the observed discrepancy between $\eta_{\mathrm{s}}$ and $\eta_{\mathrm{p}}$.

Another more likely cause of this disagreement lies in the loss of accelerated trailing bunch charge. Although limited by only using shots with the 10 % highest $Q_{\mathrm{acc}}$ at each collimator position, a systematic uncertainty may remain if there is still trailing bunch charge loss. At this point, however, it is unclear where such charge loss occurs and its exact nature would impact each measurement in different ways. For instance, the spectrometer can at best only measure the average acceleration efficiency of the trailing bunch charge that is successfully transported to the end of the plasma; extra losses of charge in the postplasma beamline would then further decrease the value measured there. On the other hand, the emission-light-based method measures the efficiency directly at the plasma location; charge loss downstream of the plasma will not affect the measurement and any changes in

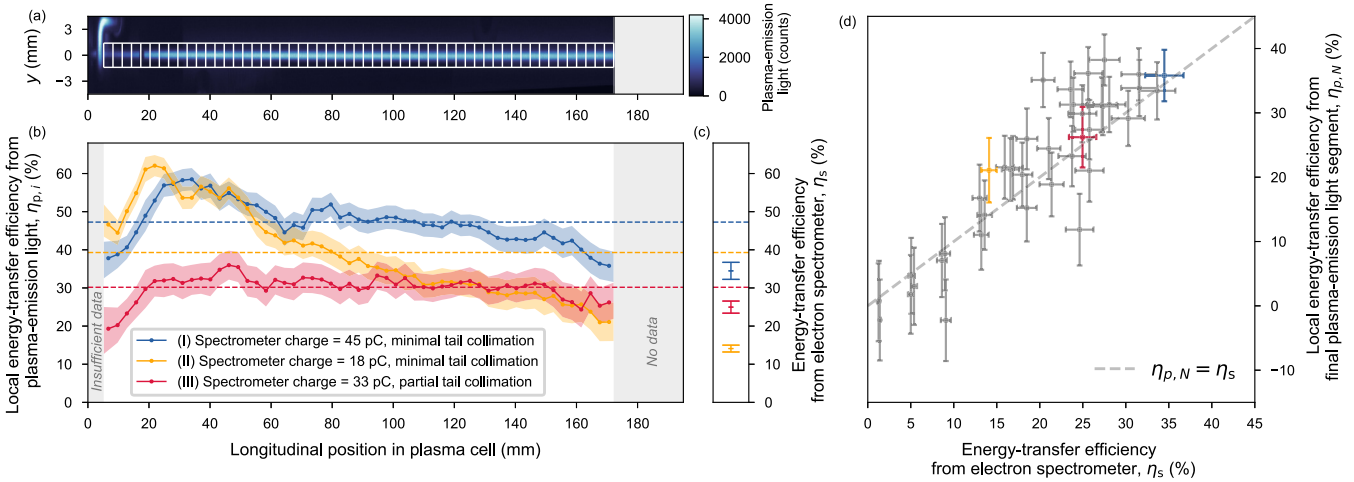



FIG. 4. (a) The plasma-emission light is separated into 3-mm-long segments (white boxes). (b) Local energy-transfer efficiency is shown as a function of position along the plasma cell. Three separate shots were considered, each with different amounts of trailing bunch charges and efficiencies measured at the spectrometer (blue, orange, and red lines). The error bands represent the uncertainty of the response curve fit for each segment, as well as the jitter of the total driver energy loss. The dashed lines represent the averages of the curves and are equal to the efficiencies calculated from the whole plasma in Fig. 3. (c) Corresponding spectrometer-based measurements of efficiency are shown. (d) Comparison of energy-transfer efficiency measured with the final segment of plasma-emission light against that measured with the spectrometer. The shots from panel (c) are highlighted with their corresponding colors.

the acceleration efficiency along the plasma will be reflected in the result. The latter point now motivates the exploitation of a key feature of the plasma-emission light signal—its spatial resolution—which suggests the possibility of longitudinally resolved energy-transfer efficiency measurements along the length of the plasma stage.

## VI. LONGITUDINALLY RESOLVED ENERGY-TRANSFER EFFICIENCY MEASUREMENTS

In order to longitudinally resolve the energy-transfer efficiency, the plasma can be divided into $N$ segments [see Fig. 4(a)]. In general, the local energy-transfer efficiency in the $i$th segment can be defined as

$$\eta_i = \frac{\Delta W_{\mathrm{acc},i}}{\Delta W_{\mathrm{dec},i}}, \tag{5}$$

where $\Delta W_{\mathrm{dec},i}$ is the localized driver energy loss and $\Delta W_{\mathrm{acc},i}$ is the localized energy gain of the trailing bunch in the $i$th segment. In order to measure this with the plasma-emission light, Eq. (5) can be written in a way analogous to Eq. (3) as

$$\eta_{\mathrm{p},i} = 1 - \frac{\Delta W_{\mathrm{wake},i}}{\Delta W_{\mathrm{dec},i}}, \tag{6}$$

where the localized remaining wake energy $\Delta W_{\mathrm{wake},i}$ can be calculated from the version of Eq. (2) for a single segment, $\Delta W_{\mathrm{wake}} = f_i^{-1}(I_{\mathrm{p},i})$, where $I_{\mathrm{p},i}$ and $f_i$ are the plasma light yield and response curve for the $i$th segment, respectively. Similarly, $\Delta W_{\mathrm{dec},i}$ can be estimated with the version of Eq. (4), where $f$ and $I_{\mathrm{p}}$ are replaced by $f_i$ and $I_{\mathrm{p},i}$. Here, it is implicitly assumed that there is negligible longitudinal movement of the plasma components, such that the light signal still reflects the local energy loss at a given position. Observations in Ref. [34] support this assumption, where for a similar experimental setup, the reacceleration of depleted electrons coincides with a localized decrease in the plasma-emission light.

The main obstacle to the direct application of Eq. (6) is the construction of the segment response curves $f_i$. Ideally, these would be derived from direct measurements of $I_{\mathrm{p},i}$ versus $\Delta W_{\mathrm{dec},i}$ with only the driver present, in a similar fashion to Fig. 2(b). However, the spectrometer can only measure the integrated driver energy loss $\Delta W_{\mathrm{dec}}$. In order to proceed, information about the relationship between $\Delta W_{\mathrm{dec}}$ and $\Delta W_{\mathrm{dec},i}$ during response curve calibration is required. Without loss of generality, one can write $\Delta W_{\mathrm{dec},i} = k_i(\Delta W_{\mathrm{dec}})\Delta W_{\mathrm{dec}}$, where $k_i(\Delta W_{\mathrm{dec}})$ describes the proportion of the total driver energy loss deposited in each segment. In general, this can be a function of $\Delta W_{\mathrm{dec}}$ itself if $\Delta W_{\mathrm{dec},i}$ varies nonlinearly with $\Delta W_{\mathrm{dec}}$ during response curve construction.

Here, the local and integrated driver energy losses are assumed to be proportional to each other. In this case, $k_i$ can still be different for each $i$, but crucially is not a function of $\Delta W_{\mathrm{dec}}$, i.e., it is a constant of proportionality for each segment. It follows that the response curve can be constructed purely from the integrated driver energy loss via $I_{\mathrm{p},i} = f_i(k_i \Delta W_{\mathrm{dec}})$. Note that here, the response curves for each segment display a similar shape to that shown in Fig. 2(b); as the values of $I_{\mathrm{p},i}$ again remain in the linear region of the curves, linear fits are once more sufficient to represent $f_i$. Although $k_i$ remains an unknown scaling factor, the assumption that it is constant for each segment means that its effect will cancel out where the response curves are used in both the numerator and denominator of Eq. (6). A more formal discussion of this assumption—and the systematic error introduced if it does not hold true—is given in the Appendix.

Figure 4(b) demonstrates a longitudinally resolved measurement of energy-transfer efficiency for three separate shots with an accelerated trailing bunch, labeled (I), (II), and

(III). Whereas shots (I) and (II) were collected with the tail collimator the furthest extracted, shot (III) has this collimator partially inserted, such that, on average, 20 pC of charge is removed from the rear of the trailing bunch. The $\eta_s$ for these shots are shown in Fig. 4(c). Differences in $\eta_s$ are mainly driven by variations in the trailing bunch charge measured at the spectrometer, where $Q_{acc} =$ (I) 45 pC, (II) 18 pC, and (III) 33 pC.

Notably, the efficiencies measured at the spectrometer for these shots are much closer to the efficiencies measured for the segment nearest to the end of the plasma, $\eta_{p,N}$, than the average efficiency measured using the emission light [dashed lines, Figs. 4(b) and 4(c)], which correspond to the $\eta_p$ values represented on the vertical axis of Fig. 3. As shown by Fig. 4(d), this is indeed a general trend. When plotting the efficiency from this last segment against the spectrometer-based efficiency for all of the data in Fig. 3, the agreement is much improved, with most points lying close to the line $\eta_s = \eta_{p,N}$.

To investigate this observation, one can examine the behavior of the curves in Fig. 4(b). The rapid initial increase in energy-transfer efficiency is likely due to a plasma-density upramp at the entrance of the cell ($\sim$0–25 mm)—a similar decrease is also expected in the downramp at the cell exit ($\sim$175–195 mm), which in this experiment was beyond the field of view of the emission light camera. Of more interest is the behavior observed between these regions, where the plasma density is expected to be approximately uniform.

Consider first the shots (I) and (II), where the efficiency decreases between 20 and 175 mm. In principle, this could be explained by an increase in the energy deposited by the driver that is not subsequently extracted by the trailing bunch. However, as suggested by Fig. 5(a) in the Appendix, the relative change in the driver energy deposition is not expected to be of this level, and is moreover expected to decrease as the drive beam undergoes, e.g., head erosion. Instead, the decrease is deemed more likely to be caused by changes in $\Delta W_{acc,i} = Q_{acc,i}\Delta E_{acc,i}$, where $\Delta E_{acc,i}$ is the electron energy gain of the trailing bunch charge $Q_{acc,i}$ present in the $i$th plasma segment.

Consider the scenario that $\Delta E_{acc,i}$ is decreasing through the middle region, while $Q_{acc,i}$ is the same in all segments as it is at the end of the plasma, $Q_{acc,N}$. In this case, where for simplicity $\Delta W_{dec,i}$ is assumed constant, it can be shown that the longitudinally averaged efficiency is $\frac{Q_{acc,N}}{\Delta W_{dec}} \sum_{i=1}^{N} \Delta E_{acc,i}$. Provided that there is also no trailing bunch charge loss in the postplasma beamline, this is equal to the efficiency measured in the spectrometer in Eq. (1). This then would lead to agreement between the longitudinally averaged efficiency from the emission light and that measured with the spectrometer—but this is not observed.

Instead, consider the situation where $\Delta E_{acc,i}$ is constant but that there is trailing bunch charge lost from the wake that then ceases to exchange energy with the plasma. The longitudinally averaged efficiency is then $\frac{\Delta E_{acc}}{\Delta W_{dec}} \frac{1}{N} \sum_{i=1}^{N} Q_{acc,i}$. Whereas this result is reflected in averaging over $\eta_{p,i}$ from the emission light, the spectrometer can only at best measure the energy-transfer efficiency for the trailing bunch at the end of the plasma; if $Q_{acc,N} < Q_{acc,i<N}$, $\eta_s$ will underestimate the true longitudinally averaged efficiency. This explains the improved agreement between $\eta_{p,N}$ and $\eta_s$ and moreover implies that the decrease in efficiency observed in the center of the plasma cell is compatible with trailing bunch charge loss.

This charge loss could be attributed to parts of the trailing bunch being transversely kicked or defocused within the plasma, which would also make charge loss in the postplasma transport more likely, leading to a further decrease in the $\eta_s$ measured in the spectrometer. Such occurrences would explain the fact that, for shots such as (II), the data points in Fig. 4(d) still lie to the left of the line $\eta_{p,N} = \eta_s$. Charge located at the back of the wake is especially susceptible to these transverse effects, which may also offer an explanation for the differing behavior of shot (III). Here, charge with a higher potential to be lost during plasma acceleration was removed from the rear of the trailing bunch via the tail collimator, resulting in an approximately uniform local efficiency profile. Moreover, this would also confirm that a changing rate of driver energy deposition—which is not affected by the removal of trailing bunch charge—is not responsible for the efficiency decrease observed for shots (I) and (II).

The previous discussion highlights a major advantage of the emission-light-based efficiency measurement. While electron spectrometers remain vital components of any plasma accelerator and are indeed required to initially construct the wake-energy-versus-plasma-light response curve [Fig. 2(b)], they can only measure the energy-transfer efficiency of the trailing bunch that is successfully transported through the plasma and postplasma beamline. The emission light measurement, on the other hand, takes place directly at the location of acceleration stage and thus accounts for trailing bunch charge that may be lost partway through or indeed after the plasma. By utilizing the spatial resolution of this diagnostic, already more insight has been gained into the in-plasma trailing bunch transport. In the future, this could include the experimental diagnosis of transverse instabilities and, for example, how they may limit high-efficiency plasma acceleration [37–39], which has proven notoriously difficult in the past.

## VII. OUTLOOK

Looking further ahead, the noninvasive nature of this method will enable online optimization and monitoring of plasma accelerators also when the trailing bunch cannot be intercepted by a spectrometer. This applies during operation in most applications, and, in particular, for multistage plasma accelerators [40,41], where separate diagnosis of the acceleration process in each stage will be crucial, but cannot be provided by a single spectrum measurement. Ultimately, this method would form part of a suite of diagnostics that would need to measure, for example, the transverse properties of the bunches. Although this would almost certainly still include screens for detailed, offline diagnosis, methods based on, e.g., betatron radiation may offer noninvasive measurements of the transverse emittance that would be complementary to the diagnostic presented here [42].

As discussed in Sec. VI, coupling of the trailing bunch charge into the wake is a key aspect of the acceleration process that could be monitored and optimized with the

emission-light-based diagnostic. Furthermore, as mentioned in Sec. IV, the ability to diagnose the efficiency of a plasma stage without the need for a trailing bunch measurement would also mean that spectrometer measurements could instead prioritize the measurement of $\Delta W_{\mathrm{dec}}$, yielding potentially more accurate efficiencies than can be provided by measuring both driver and trailing bunches with the same spectrometer. Future work could also aim to better understand the physics of the plasma-emission light, where spectrally and/or temporally resolved measurements could yield yet more information about the energy-transfer processes and more generally contribute to an understanding of the long-term plasma evolution—a key area of research within the field.

In summary, a method for measuring the energy-transfer efficiency in a plasma accelerator was presented, using excess plasma-emission light to infer the energy remaining in the wake. This enabled the longitudinally resolved measurement of the local energy-transfer efficiency evolution throughout the acceleration process. We foresee that this simple, noninvasive technique can provide deeper understanding and more reliable operation of plasma-accelerator stages—especially important as the field looks toward multiple stages and applications.

## ACKNOWLEDGMENTS

The authors would like to thank M. Dinter, S. Karstensen, S. Kottler, K. Ludwig, F. Marutzky, A. Rahali, V. Rybnikov, A. Schleiermacher, the FLASH management, and the DESY FH, FS, M, and V divisions for their scientific, engineering, and technical support. This work was supported by Helmholtz ARD, Helmholtz ATHENA and the Helmholtz IuVF ZT-0009 programme, as well as the Maxwell computational resources at DESY. L.B. was supported by an Engineering and Physical Sciences Research Council (EPSRC) Studentship. B.H. was supported by the European Research Council (ERC) under the European Union's Horizon 2020 Research and Innovation Programme (NeX-ource: Next-generation Plasma-based Electron Beam Sources for High-brightness Photon Science, ERC Grant Agent No. 865877) and by the STFCPWFA-FEL Programme Grant No. ST/S006214/1.

## DATA AVAILABILITY

The data that support the findings of this article are not publicly available upon publication because it is not technically feasible and/or the cost of preparing, depositing, and hosting the data would be prohibitive within the terms of this research project. The data are available from the authors upon reasonable request.

## APPENDIX: ASSUMPTION ON THE RELATION BETWEEN LOCALIZED AND INTEGRATED TOTAL DRIVER ENERGY LOSS

In order to understand the possible form of $k_i(\Delta W_{\mathrm{dec}})$ and its implications for longitudinally resolved efficiency measurements, simulations were performed of the driver-only energy loss through the 195-mm-long plasma cell using the three-dimensional quasistatic particle-in-cell (PIC) code HiPACE++ [43]. Similar to what was shown in Ref. [34], the plasma profile was approximated as a 145-mm-long flattop with plateau plasma density $5.6 \times 10^{15}\,\mathrm{cm}^{-3}$ that has Gaussian ramps extending to the exits of the 195-mm-long plasma cell, with external ramps that rapidly decay to zero beyond this. For simplicity, the driver was simulated as a Gaussian in all directions with a charge of 400 pC, mean energy of 1045 MeV, peak current of 1 kA, and symmetric beta functions with 10 mm vacuum waists located at the start of the plasma flattop. Three sets of simulations with symmetric normalized transverse driver emittances of $\epsilon_{\mathrm{n}} = 1$, 20, and 40 mm mrad were run. Changing the emittance varies the amount of driver charge effectively coupled into the wake, along with how the wake evolves. This allows one to test the effect of differing driver energy loss behavior along the plasma. In each case, 13 simulations were performed, each with progressively more charge removed from the rear of the driver, emulating the tail collimator scan performed in the experiment. By extracting $\Delta W_{\mathrm{dec},i}$ and $\Delta W_{\mathrm{dec}}$ for each driver charge case, the relationship between the two could be determined.

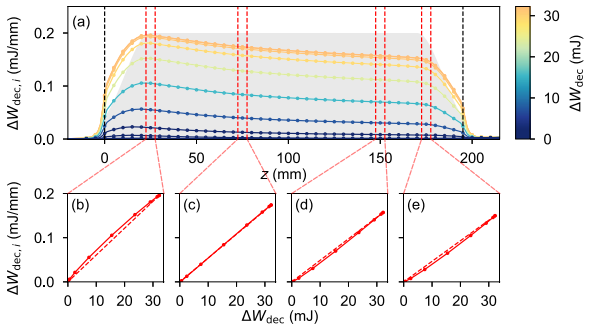



FIG. 5. (a) Simulated local driver energy loss (colored lines and points) for the case $\epsilon_{\mathrm{n}} = 40$ mm mrad, for different driver charges. The color scale shows the integrated driver energy loss for each simulation. A gray shaded profile shows the plasma profile shape, while the black vertical dashed lines show the physical extent of the 195-mm-long cell. The relationship between the local and integrated driver energy losses is shown for selected segments (dashed boxes) in panels (b)–(e).

Figure 5 demonstrates the results of the set of these simulations for the $\epsilon_{\mathrm{n}} = 40$ mm mrad case. As driver bunch charge is introduced, both the local and integrated energy loss increase [see Fig. 5(a)]. Observe that in this case, the driver energy is lost at a varying rate across the plasma, even in the uniform flattop region. This is a consequence of driver head erosion, resulting in a changing wakefield strength as the bunch propagates. It is, however, the relationship between $\Delta W_{\mathrm{dec}}$ and $\Delta W_{\mathrm{dec},i}$ that is of the most importance here, which is examined for four example segments in Figs. 5(b)–5(e). Generally, the relation is close to, but not exactly, linear. This is illustrated by the fact that the points and the line connecting them (solid red) do not always coincide with the line connecting the first and last points (dashed red). As a more concrete quantification of the degree of linearity of this relation, the Pearson correlation coefficient $r$ can be calculated for the two quantities; across the segments, $0.998 < r < 1$, where $r = 1$ represents a perfectly linear relation. In terms of the factor $k_i(\Delta W_{\mathrm{dec}})$, $r \neq 1$

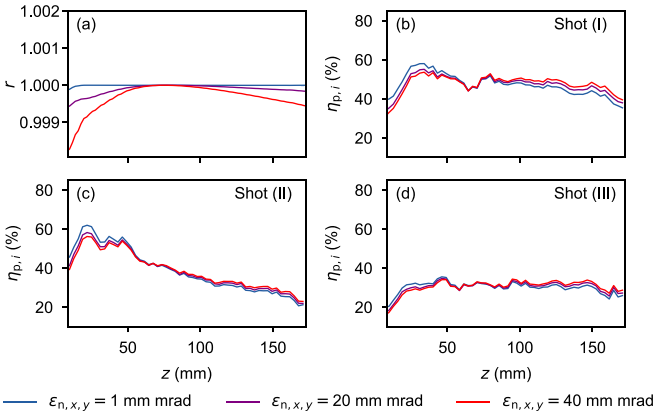



FIG. 6. (a) Pearson correlation coefficients $r$ between $\Delta W_{\mathrm{dec}}$ and $\Delta W_{\mathrm{dec},i}$ are plotted for the $\epsilon_{\mathrm{n}} = 1$ (blue), 20 (purple), and 40 mm mrad (red) cases. In the panels (b)–(d), the same shots (I)–(III) are shown as in Fig. 4, respectively. In each panel, the three lines represent the longitudinally resolved efficiency for the given shot recalculated for the three different emittance cases, where the same color code is used as in panel (a). For clarity, the error bands on these lines are not shown, but are of a similar size to those on the data in Fig. 4.

implies that the factor is not constant for a given segment during the driver charge scan and can vary with $\Delta W_{\mathrm{dec}}$. In order to assess the potential impact of this effect on the results shown in Fig. 4, we convert $\Delta W_{\mathrm{dec}}$ measured in experiment to $\Delta W_{\mathrm{dec},i}$ by interpolating between the points shown in Figs. 5(b)–5(e). From this, the local response curves $f_i$ can be constructed. This process can be repeated for each emittance case, each time recalculating the longitudinally resolved efficiency via Eq. (6) for the same experimental data as in Fig. 4.

The results of this analysis are displayed in Fig. 6 for the three emittance cases. As shown by Fig. 6(a), the nonlinearity of the relationship between $\Delta W_{\mathrm{dec}}$ and $\Delta W_{\mathrm{dec},i}$ in general varies as the beam propagates. The extreme case of $\epsilon_n = 40$ mm mrad (red) experiences this effect the most severely. On the other hand, the idealized case of $\epsilon_n = 1$ mm mrad (blue)—where there is negligible wake evolution—displays no evidence of this behavior. In the latter case, the assumption used in the main text—that the relationship between $\Delta W_{\mathrm{dec}}$ and $\Delta W_{\mathrm{dec},i}$ is linear during response curve construction—holds true, while it is violated in cases where $r < 1$. Indeed, this is reflected when calculating the local energy-transfer efficiency. For each emittance case, the longitudinally resolved response curves are constructed and applied using Eq. (6) to the same three shots considered in Fig. 4, where the results are shown in Figs. 6(b)–6(d) correspond to shots (I), (II), and (III), respectively. For the $\epsilon_n = 1$ mm mrad case (blue), the same $\eta_{\mathrm{p},i}$ is recovered as when using the assumption in the main manuscript. Violations of this assumption lead to a systematic change in the efficiency values across the plasma extent. In these cases, the efficiency at the beginning of the plasma decreases, whereas toward the end it increases. Although this systematic error remains on the level of a few percentage points for most of the cell extent, in the worst case of $\epsilon_n = 40$ mm mrad, it can be up to 8 percentage points in the region where $r$ is the lowest. This, however, represents an extreme and unlikely scenario for this experiment, with an artificially high emittance used purely to demonstrate the impact of a nonideal driver on longitudinal efficiency calculations. Although detailed driver emittance measurements were unavailable for the data presented in this paper, characterization of similar beams in Ref. [15], for example, only measured horizontal emittances as high as 20 mm mrad for slices at the head of the driver, which are also in general lower in the vertical direction. As such, even the $\epsilon_{\mathrm{n}} = 20$ mm mrad case can reasonably be expected to overestimate this effect.


[1] W. P. Leemans, B. Nagler, A. J. Gonsalves, Cs. Tóth, K. Nakamura, C. G. R. Geddes, E. Esarey, C. B. Schroeder, and S. M. Hooker, GeV electron beams from a centimetre-scale accelerator, Nat. Phys. **2**, 696 (2006).

[2] M. J. Hogan, C. D. Barnes, C. E. Clayton, F. J. Decker, S. Deng, P. Emma, C. Huang, R. H. Iverson, D. K. John-son, C. Joshi, T. Katsouleas, P. Krejcik, W. Lu, K. A. Marsh, W. B. Mori, P. Muggli, C. L. OConnell, E. Oz,R. H. Siemann, and D. Walz, Multi-GeV energy gain in a plasma-wakefield accelerator, Phys. Rev. Lett. **95**, 054802 (2005).

[3] I. Blumenfeld, C. E. Clayton, F.-J. Decker, M. J. Hogan, C. Huang, R. Ischebeck, R. Iverson, C. Joshi, T. Kat-souleas, N. Kirby, W. Lu, K. A. Marsh, W. B. Mori, P. Muggli, E. Oz, R. H. Siemann, D. Walz, and M. Zhou, Energy doubling of 42 GeV electrons in a metre-scale plasma wakefield accelerator, Nature (London) **445**, 741 (2007).

[4] T. Tajima and J. M. Dawson, Laser electron accelerator, Phys. Rev. Lett. **43**, 267 (1979).

[5] P. Chen, J. M. Dawson, R. W. Huff, and T. Katsouleas, Acceleration of electrons by the interaction of a bunched electron beam with a plasma, Phys. Rev. Lett. **54**, 693 (1985).

[6] R. D. Ruth, A. W. Chao, P. L. Morton, and P. B. Wilson, A plasma wake field accelerator, Part. Accel. **17**, 171 (1985).

[7] B. Foster, R. D'Arcy, and C. A. Lindstrøm, A hybrid, asymmetric, linear Higgs factory based on plasma-wakefield and radio-frequency acceleration, New J. Phys. **25**, 093037 (2023).

[8] S. van der Meer, Improving the power efficiency of the plasma wakefield accelerator, CLIC Note, No. 3, 1985.

[9] P. Chen, J. J. Su, J. M. Dawson, K. L. F. Bane, and P. B. Wilson, Energy transfer in the plasma wake-field accelerator, Phys. Rev. Lett. **56**, 1252 (1986).

[10] K. V. Lotov, Efficient operating mode of the plasma wakefield accelerator, Phys. Plasmas **12**, 053105 (2005).

[11] T. Katsouleas, S. Wilks, P. Chen, J. M. Dawson, and J. J. Su, Beam loading in plasma accelerators, Part. Accel. **22**, 81 (1986).

[12] M. Tzoufras, W. Lu, F. S. Tsung, C. Huang, W. B. Mori, T. Katsouleas, J. Vieira, R. A. Fonseca, and L. O. Silva, Beam loading in the nonlinear regime of plasma-based acceleration, Phys. Rev. Lett. **101**, 145002 (2008).

[13] M. Litos *et al.*, High-efficiency acceleration of an electron beam in a plasma wakefield accelerator, Nature (London) **515**, 92 (2014).

[14] M. Litos, E. Adli, J. M. Allen, W. An, C. I. Clarke, S. Corde, C. E. Clayton, J. Frederico, S. J. Gessner, S. Z. Green, M. J. Hogan, C. Joshi, W. Lu, K. A. Marsh, W. B. Mori, M. Schmeltz, N. Vafaei-Najafabadi, and V. Yakimenko, 9 GeV energy gain in a beam-driven plasma wakefield accelerator, Plasma Phys. Control. Fusion **58**, 034017 (2016).

[15] C. A. Lindstrøm, J. M. Garland, S. Schröder, L. Boul-ton, G. Boyle, J. Chappell, R. D'Arcy, P. Gonzalez, A. Knetsch, V. Libov, G. Loisch, A. Martinez de la Ossa, P. Niknejadi, K. Pöder, L. Schaper, B. Schmidt, B. Sheeran, S. Wesch, J. Wood, and J. Osterhoff, Energy-spread preservation and high efficiency in a plasma-wakefield accelerator, Phys. Rev. Lett. **126**, 014801 (2021).

[16] S. Steinke, J. van Tilborg, C. Benedetti, C. G. R. Geddes, C. B. Schroeder, J. Daniels, K. K. Swanson, A. J.Gonsalves, K. Nakamura, N. H. Matlis, B. H. Shaw, E. Esarey, and W. P. Leemans, Multistage coupling of independent laser-plasma accelerators, Nature (London) **530**, 190 (2016).

[17] C. A. Lindstrøm, Staging of plasma-wakefield accelerators, Phys. Rev. Accel. Beams **24**, 014801 (2021).

[18] E. Oz, C. D. Barnes, C. E. Clayton, F. J. Decker, S. Deng, M. J. Hogan, C. Huang, R. Iverson, D. K. Johnson, C. Joshi, T. Katsouleas, P. Krejcik, W. Lu, K. A. Marsh, P. Muggli, C. O'Connell, and D. Walz, Optical diagnostics for plasma wakefield accelerators, AIP Conf. Proc. **737**, 708 (2004).

[19] C. Zhang *et al.*, Correlations between x-rays, visible light and drive-beam energy loss observed in plasma wakefield acceleration experiments at FACET-II, J. Plasma Phys. **90**, 965900401 (2024).

[20] P. Scherkl *et al.*, Plasma photonic spatiotemporal synchronization of relativistic electron and laser beams, Phys. Rev. Accel. Beams **25**, 052803 (2022).

[21] E. Adli, C. A. Lindstrøm, J. Allen, C. Clarke, J. Fred-erico, S. Gessner, S. Green, M. J. Hogan, M. D. Litos, B. O'Shea, V. Yakimenko, W. An, C. E. Clayton, K. A. Marsh, W. B. Mori, C. Joshi, N. Vafaei-Najafabadi, S. Corde, and W. Lu, Long-range attraction of an ultrarelativistic electron beam by a column of neutral plasma, New J. Phys. **18**, 103013 (2016).

[22] V. Lee, R. Ariniello, D. Storey, S. Corde, C. Emma, S. Gessner, M. Hogan, A. Knetsch, N. Majernik, B. O'Shea, I. Rajkovic, and M. Litos, Precision alignment and tolerance of a plasma wakefield accelerator in a laser-ionized plasma source, Phys. Rev. Accel. Beams **29**, 041001 (2026).

[23] V. Lee, R. Ariniello, C. Doss, K. Wolfinger, P. Stoltz, C. Hansel, S. Gessner, J. Cary, and M. Litos, Temporal evolution of the light emitted by a thin, laser-ionized plasma source, Phys. Plasmas **31**, 013104 (2024).

[24] J. Mezger, M. Bergamaschi, L. Ranc, A. Sublet, J. Pucek, M. Turner, A. Clairembaud, and P. Muggli, Implementation of light diagnostics for wakefields at AWAKE, Nucl. Instrum. Methods Phys. Res. Sect. A **1075**, 170426 (2025).

[25] R. D'Arcy *et al.*, FLASHForward: Plasma wakefield accelerator science for high-average-power applications, Phil. Trans. R. Soc. A **377**, 20180392 (2019).

[26] S. Schreiber and B. Faatz, The free-electron laser FLASH, High Power Laser Sci. Eng. **3**, e20 (2015).

[27] P. González Caminal *et al.*, Beam-based commissioning of a novel *X*-band transverse deflection structure with variable polarization, Phys. Rev. Accel. Beams **27**, 032801 (2024).

[28] S. Schröder, K. Ludwig, A. Aschikhin, R. D'Arcy, M. Dinter, P. Gonzalez, S. Karstensen, A. Knetsch, V. Li-bov, C. A. Lindstrøm, F. Marutzky, P. Niknejadi, A. Rahali, L. Schaper, A. Schleiermacher, B. Schmidt, S. Thiele, A. de Zubiaurre Wagner, S. Wesch, and J. Os-terhoff, Tunable and precise two-bunch generation at FLASHForward, J. Phys.: Conf. Ser. **1596**, 012002 (2020).

[29] C. A. Lindstrøm, R. D'Arcy, M. J. Garland, P. Gonzalez, B. Schmidt, S. Schröder, S. Wesch, and J. Osterhoff, Matching small $\beta$ functions using centroid jitter and two beam position monitors, Phys. Rev. Accel. Beams **23**, 052802 (2020).

[30] D. J. Spence and S. M. Hooker, Investigation of a hydrogen plasma waveguide, Phys. Rev. E **63**, 015401(R) (2000).

[31] J. M. Garland, G. Tauscher, S. Bohlen, G. J. Boyle, R. D'Arcy, L. Goldberg, K. Põder, L. Schaper, B. Schmidt, and J. Osterhoff, Combining laser interferometry and plasma spectroscopy for spatially resolved high- sensitivity plasma density measurements in discharge capillaries, Rev. Sci. Instrum. **92**, 013505 (2021).

[32] M. A. Gigosos, M. A. González, and V. Cardeñoso, Computer simulated Balmer-alpha, -beta and -gamma Stark line profiles for non-equilibrium plasmas diagnostics, Spectrochim. Acta, Part B **58**, 1489 (2003).

[33] A. Buck, K. Zeil, A. Popp, K. Schmid, A. Jochmann, S. D. Kraft, B. Hidding, T. Kudyakov, C. M. S. Sears, L. Veisz, S. Karsch, J. Pawelke, R. Sauerbrey, T. Cowan, F. Krausz, and U. Schramm, Absolute charge calibration of scintillating screens for relativistic electron detection, Rev. Sci. Instrum. **81**, 033301 (2010).

[34] F. Peñna, C. A. Lindstrøm, J. Beinortaitė, J. Björklund Svensson, L. Boulton, S. Diederichs, B. Foster, J. M. Gar-land, P. Gonz'alez Caminal, G. Loisch, S. Schröder, M. Th'evenet, S. Wesch, J. C. Wood, J. Osterhoff, and R. D'Arcy, Energy depletion and re-acceleration of driver electrons in a plasma-wakefield accelerator, Phys. Rev. Res. **6**, 043090 (2024).

[35] R. Zgadzaj, T. Silva, V. K. Khudyakov, A. Sosedkin, J. Allen, S. Gessner, Z. Li, M. Litos, J. Vieira, K. V. Lotov, M. J. Hogan, V. Yakimenko, and M. C. Downer, Dissipation of electron-beam-driven plasma wakes, Nat. Commun. **11**, 4753 (2020).

[36] R. D'Arcy, J. Chappell, J. Beinortaite, S. Diederichs, G. Boyle, B. Foster, M. J. Garland, P. Gonzalez Caminal, C. A. Lindstrøm, G. Loisch, S. Schreiber, S. Schröder, R. J. Shalloo, M. Thévenet, S. Wesch, M. Wing, and J. Os-terhoff, Recovery time of a plasma-wakefield accelerator, Nature (London) **603**, 58 (2022).

[37] V. Lebedev, A. Burov, and S. Nagaitsev, Efficiency versus instability in plasma accelerators, Phys. Rev. Accel. Beams **20**, 121301 (2017).

[38] S. S. Baturin, On "Efficiency versus instability in plasma accelerators," arXiv:2010.01046.

[39] O. G. Finnerud, C. A. Lindstrøm, and E. Adli, Parametric mapping of the efficiency–instability relation in plasma-wakefield accelerators, Phys. Rev. Accel. Beams **28**, 071301 (2025).

[40] S. Pei, M. J. Hogan, T. O. Raubenheimer, A. Seryi, H. H. Braun, R. Corsini, and J. P. Delahaye, Conceptual design of the drive beam for a PWFA-LC, in *Proceedings of PAC09*, Vancouver, BC, Canada (JACoW, Geneva, 2009), p. 2682.

[41] E. Adli, J.-P. Delahaye, S. J. Gessner, M. J. Hogan, T. O. Raubenheimer, W. An, C. Joshi, and W. B. Mori, A beam

driven plasma-wakefield linear collider: From Higgs factory to multi-TeV, arXiv:1308.1145.

[42] P. San Miguel Claveria *et al.*, Betatron radiation and emittance growth in plasma wakefield accelerators, Phil. Trans. R. Soc. A **377**, 20180173 (2019).

[43] S. Diederichs, C. Benedetti, A. Huebl, R. Lehe, A. Myers, A. Sinn, J.-L. Vay, W. Zhang, and M. Thévenet, HiPACE++: A portable 3D quasi-static particle-in-cell code, Comput. Phys. Commun. **278**, 108421 (2022).